Experimental and Molecular Pathology 144 (2025) 105011

Contents lists available at ScienceDirect

Experimental and Molecular Pathology

journal homepage: www.elsevier.com/locate/yexmp

Wharton's jelly-derived nanovesicles for targeting intervertebral disc degeneration

Letizia Penolazzi [a], Alice Zaramella [b,c], Anna Chierici [a], Paola Bisaccia [b,c], Maria Pina Notarangelo [a], Anna Maria Tolomeo [c,d], Elisabetta Lambertini [e], Anna Alessia Saponaro [f,g], Tommaso Colangelo [f,g], Michela Pozzobon [b,c,*], Roberta Piva [a,*]

[a] Department of Neuroscience and Rehabilitation, University of Ferrara, Ferrara, Italy
[b] Department of Women's and Children's Health, University of Padova, Padova, Italy
[c] Institute of Pediatric Research Città della Speranza, Padova, Italy
[d] Department of Cardiac Thoracic and Vascular Sciences and Public Health, University of Padova, Italy
[e] Laboratorio centralizzato di ricerca preclinica, University of Ferrara, 44121 Ferrara, Italy
[f] C.R.E.A.T.E - Center for Research and Innovation in Medicine, Dept. of Medical and Surgical Sciences, University of Foggia, Italy
[g] Cancer Cell Signaling Unit, Fondazione IRCCS "Casa Sollievo della Sofferenza", San Giovanni Rotondo, Foggia, Italy

ARTICLE INFO

Keywords:
Matrix vesicles
Human intervertebral disc
Decellularized Wharton's jelly matrix
Discogenic phenotype

ABSTRACT

The present study was designed to characterize the matrix-bound nanovesicles (MBVs) in decellularized Wharton's jelly matrix (DWJ). We have previously used DWJ as a biomaterial demonstrating its efficacy in restoring the functional properties of human intervertebral disc (IVD) cells lost following degeneration (IDD), for which there is currently no cure.

MBVs were isolated by ultracentrifugation from DWJ, characterized by transmission electron microscopy, nanoparticle tracking assay, and surface marker expression. MBVs uptake into cells was assessed by CalceinAM labeling. Nitric oxide production was evaluated by Griess assay. The response of IVD cells was assessed by cell motility (wound scratch assay) and protein expression (immunocytochemistry). MBVs were subjected to human growth factors array to evaluate different growth factors and global miRNA profiling (obtained from miRNA libraries, sequencing-NextSeq system and the GeneGlobe Data Analysis).

MBVs were readily internalized by cells without affecting the viability. MBVs suppressed the acquisition of the M1 phenotype in LPS-stimulated macrophages, positively influence the cell migration of IVD cells and the expression of molecular markers associated with the restoration of the chondrocyte-like phenotype. A preliminary analysis of growth factor content and miRNA expression profiling suggest that MBVs carry a cargo functionally relevant for the IVD cell metabolism.

The discovery of MBVs in DWJ leads to considering them as an integral component of DWJ-based scaffolds designed to repair or regenerate a damaged tissue. The pro-discogenic properties of MBVs demonstrate that there are grounds for expanding the study of DWJ-derived MBVs for potential therapeutic applications in the treatment of IDD.

1. Introduction

Wharton's Jelly (WJ) is a special mucous connective tissue located within the umbilical cord which, thanks to its unique molecular organization, and its biological and mechanical properties, is garnering increasing attention as a potential biological scaffold (Jadalannagari

Abbreviations: MBVs, Matrix-Bound Nanovesicles; DWJ, Decellularized Wharton's Jelly matrix; IVD, Intervertebral Disc; IDD, Intervertebral Disc Degeneration; ECM, Extracellular Matrix; DMEM, Dulbecco's Modified Eagle Medium; RT, room temperature; TEM, transmission electron microscopy; NTA, Nanoparticle Tracking Analysis; TRPS, Tunable Resistive Pulse Sensing (TRPS); NO, Nitric Oxide; LPS, Lipopolysaccharide; Dil, 1, 1′-dioctadecyl-3, 3, 3′, 3′-tetramethyl indocarbocyanine perchlorate; PBS, Phosphate-Buffered Saline; DAPI, diamidino-2-phenylindole; miRNA, microRNA; MSigDB, Molecular Signature Database; RT-qPCR, Reverse Transcription-Quantitative Polymerase Chain Reaction; ANOVA, Analysis of Variance; CD, Cluster of Differentiation..

* Corresponding authors.
E-mail addresses: michela.pozzobon@unipd.it (M. Pozzobon), piv@unife.it (R. Piva).

https://doi.org/10.1016/j.yexmp.2025.105011
Received 16 July 2025; Received in revised form 12 November 2025; Accepted 17 November 2025
Available online 29 November 2025

et al., 2017). To date, effective cell removal procedures have been developed to produce a decellularized Wharton's jelly matrix (DWJ) that maintains the original architecture of the extracellular matrix (ECM) without alterations in the physical and mechanical properties (Converse et al., 2018). Furthermore, the decellularization process preserves the bioactive components present in the native WJ (matrix-bound cytokines, enzyme inhibitors, and growth factors such as FGFs, EGF, PDGF, and IGF-1) ensuring that a potentially suitable microenvironment is provided for cells to grow, migrate and differentiate (Dubus et al., 2022). The DWJ, like many other decellularized ECMs, can also be combined with different kinds of supplementals to optimize their efficacy in tissue repair and regeneration through the development of specifically tailored composite scaffolds. There is considerable evidence demonstrating the versatility of the DWJ, particularly its potential use as a scaffold for cartilage tissue engineering, due to the presence of components similar to the ECM of articular cartilage and anabolic factors that promote chondrocyte differentiation (Safari et al., 2019).

We recently demonstrated that human DWJ alone or in a mixture with alginate and gelatin restored functional properties of human intervertebral disc (IVD) cells lost following disc tissue degeneration and inflammation (Penolazzi et al., 2024). IVD cells are an heterogenous cellular population including notochordal cells, chondrocyte-like cells and their progenitors that produce a specific ECM whose integrity is heavily compromised when IVD degeneration (IDD) occurs (Taylor and Erwin, 2024; Zhang et al., 2022). To understand the mechanisms by which the DWJ induced beneficial effects on human degenerated IVD cells and optimize its potential use we are looking in particular at the communication system through vesicles. This comes from previous scanning and transmission electron microscopic analysis that revealed the presence of numerous extracellular vesicles (EVs) in the microenvironment created by the DWJ alone and also with the IVD cells combined with it (Penolazzi et al., 2022). In particular, we aimed to study the properties of the so-called matrix-bound nanovesicles (MBVs). The MBVs have been recently identified (Piening and Wachs, 2023; Huleihel et al., 2016; Turner et al., 2022). However, information on their characterization and how they act remains insufficient when compared with nanovesicles, like exosomes and microvesicles (Raposo and Stoorvogel, 2013) that come from cells. This is mainly due to the difficulty in obtaining them as they are strongly harnessed to structural components of ECM. So far, researchers have highlighted that MBVs differ from other vesicles for different markers and cargo (various miRNAs, proteins, and lipids) (Kobayashi et al., 2022). Although MBVs have so far been isolated from only a few ECM sources, there is no doubt that their content is tissue-specific and recapitulates the biological activity of the parent ECM (Turner et al., 2022). Regarding the biological potential, much remains to be understood, however, it is reasonable to assign MBVs roles in matrix homeostasis, cell signaling, and tissue remodeling. Consequently, the discovery of these nanovesicles leads to considering them as an integral and functional component of ECM bioscaffolds designed to repair or regenerate a damaged tissue (Huleihel, 2016; Debnath et al., 2023). Starting from these premises, the present study was designed to identify the presence of MBVs in human DWJ for the following main reasons. In principle, we aimed to improve the understanding of the ways underlying the action exerted by DWJ to fully exploit its regenerative potential. Secondly, our interest in contributing to the development of innovative therapies to counteract IDD led us to study potential pro-discogenic molecules preserved after decellularization of Wharton's jelly and present in the nanovesicle cargo.

It is worth pointing out that IDD, caused by physiological aging, injury, or trauma, affects approximately 80 % of the world's population but, to date, remains without a cure (Samanta et al., 2023). Currently, traditional therapeutic strategies, surgical and non-surgical, focus on resolving symptoms without promoting IVD regeneration at the cellular level and, therefore, do not reverse the progression of the disease (Mohd Isa et al., 2022). Recent progress on biomaterials based on decellularized ECM and on products derived from it such as MBVs are making it possible to address important challenges also in the field of regenerative medicine for the IVD (Elmounedi et al., 2024). One of these challenges is to ensure the efficacy of alternative therapeutic options based on bioactive molecules whose stability may be reduced due to the harsh microenvironment of the degenerated disc (hypoxia, acid pH, inflammation and nutrient scarcity). In this regard, the intriguing idea is that potential immunomodulatory, anti-inflammatory and discogenic molecules normally entrapped in the WJ or in the MBVs could be protected for the necessary time and then properly released in order to induce the recovery of lost biological activities by the damaged IVD. Here, MBVs from DWJ were isolated, characterized, and monitored for their cytocompatibility and potential to restore the healthy phenotype of IVD cells. Together with a preliminary investigation of the molecular signature of specific growth factors and miRNAs present in MBVs from DWJ, our data provide insights into potential new treatments for IDD.

2. Materials and methods

2.1. Decellularized Wharton's jelly (DWJ) generation

Human umbilical cords (all from natural deliveries) were collected from ten newborns after mothers' understanding and written informed consent and approval of the Ethics Committee of the University of Ferrara and S. Anna Hospital (protocol no. 061199/AOUFe). Briefly, the cord was rinsed several times with sterile phosphate-buffered saline (PBS), and a single piece (about 10 cm) was dissected, after separating the epithelium along its length, to expose the underlying Wharton's jelly. The soft gel tissue was then finely chopped. Several fragments of Wharton's jelly were subjected to detergent-enzymatic treatment (DET): samples were washed 2 times in PBS and then placed in deionized water at 4 °C for 24 h, 4 % sodium deoxycholate (Merck KGaA, Darmstadt, Germany) at room temperature (RT) for 4 h, and 45 kU/mL DNase-I (Merck KGaA) in 1 M NaCl at RT for 3 h. Samples were lyophilized and used for MBVs isolation.

2.2. IVD cell isolation

Human lumbar IVD tissues were collected as surgical waste from 4 patients undergoing surgical discectomy (2 males aged 52 and 31, Pfirrman grade 4 and 5 respectively; 2 females aged 35 and 50, both Pfirrmann grade 4). This study was approved by the Ethics Committee of the University of Ferrara and University S. Anna Hospital (protocol no. 160998/AOUFe), and written informed consent was obtained from each patient (in full accordance with the Declaration of Helsinki). Nucleus pulposus tissue from each sample was macroscopically dissected from the annulus fibrosus and digested using 1 mg/mL type IV collagenase for 5 h at 37 °C in DMEM HG/Ham's F12. Cell suspension was filtered through a Falcon™ 70 μm nylon cell strainer (BD Biosciences, Franklin Lakes, NJ, United States). Subsequently, the cells were centrifuged at 300 xg for 10 min at RT, resuspended in a basal medium [DMEM HG/Ham's F12 containing 10 % fetal calf serum (FCS), 100 mg/mL of streptomycin, 100 U/mL of penicillin, and 1 % glutamine], seeded in polystyrene culture plates at a density of 10,000 cells/cm^2 and subcultured up to passage 3 (Penolazzi et al., 2018) at 37 °C with 5 % CO_2 and 80 % humidity. Cells from different patients were not pooled but used individually for the experiments below reported.

2.3. Matrix-bound vesicles (MBVs) isolation

Lyophilized DWJ (100 mg) was solubilized by treatment with collagenase type IA (≥125 U/ mg, 0.1 mg/mL) in 10 mL of enzymatic buffer: 50 mM Tris HCl (pH 7.5), 150 mM NaCl and 5 mM $CaCl_2$. The mixture was vortexed (10 s, max speed), incubated for 16 h at RT under constant agitation, and then treated with hyaluronidase type I—S (≥400 U/mg, 30 U/mL) for 15 min at 37 °C, always in constant agitation. Immediately following solubilization, the sample was centrifuged

sequentially at 2500 x*g* (10 min, 4 °C) and 10,000 x*g* (30 min, 3 times, 4 °C). The supernatant was collected and centrifuged at 100,000 x*g* for 70 min at 4 °C (Beckman Avanti J-HC, ultracentrifuge, Beckman Coulter, CA, USA), filtered with 0.22 μm pore filters. Samples diluted in PBS were stored at −80 °C until further use.

2.4. MBVs characterization and quantification

MACSPlex exosome kit (Miltenyi Biotec) was used for antigen characterization following manufacturer's instructions, optimizing the analysis through overnight incubations. The kit is specifically designed for nanoparticle analysis, enabling the detection of surface markers on EV, while excluding cells through the use of the selective isolation method applied. The kit includes a cocktail of 39 distinct fluorescently labeled bead populations - 37 targeting specific EV surface epitopes and 2 serving as isotype controls.

Particle concentration and size distribution were also analyzed, after thawing, by Nanoparticle tracking analysis (NTA) and tunable resistive pulse sensing (TRPS) technology.

NTA was performed using Nanosight™ NS500 instruments (Malvern Instruments, Amesbury, UK).

TRPS technology was performed using qNano (Izon Science, Christchurch, New Zealand) instrument. MBVs samples were diluted 1:5 in PBS and were loaded over NP150 membrane (Izon Science).

We have submitted all relevant data of our experiments to the EV-TRACK knowledgebase (EV-TRACK ID: EV250080) (EV-TRACK Consortium, 2017).

2.5. Transmission Electron microscopy

MBVs droplets were placed on carbon-coated grids for 20 min, then fixed with 2 % formaldehyde/1 % glutaraldehyde buffered solution (pH 7.4) for 20 min. After washing with distilled water and drying them, the grids were dried and stained with 0.5 % uranyl acetate for 10 min at RT.

The grids were dried and then the images were acquired with a Talos L120C G2 Transmission Electron Microscope (Thermo Fisher Scientific, MA, USA). DWJ samples were araldite embedded (Merck KGaA, Darmstadt, Germany) and the ultra-thin sections of a selected area were contrasted with uranyl acetate lead citrate, as previously reported (Penolazzi et al., 2023).

2.6. Griess assay

NO production was evaluated in the culture medium by Griess assay following a previously published protocol (Malvicini et al., 2022). Briefly, this reaction was used to indirectly detect nitric oxide (NO) by measuring one of its stable oxidation products, nitrites (NO_2^-). For this purpose, RAW 264.7 cells (2×10^4 cells/well) were seeded on 96-well plates and exposed for 24 h to different MBVs doses (1×10^8, 5×10^8, 1×10^9, and 5×10^9) in the presence of LPS (lipopolysaccharide) 10 ng/mL (Merck KGaA). Dexamethasone 1 g/mL was used as a positive control due to its potent anti-inflammatory activity. The amount of (NO_2^-) was determined by spectrophotometer (540 nm) and evaluated as μM concentration by using a sodium NO_2^- standard curve. The effect of MBVs was expressed in term of inhibition (%) of nitrite production in LPS-stimulated cells.

2.7. MBVs labeling and uptake by cells

RAW 264.7 macrophage cell line and IVD cells were separately incubated with labeled 1×10^9 MBVs to verify MBVs uptake into the cells.

Calcein AM labeling. 4×10^4 cells were seeded in 24-well plate. Once cells were attached, MBVs and 5 μL of 1 M Calcein AM (component A, Thermo fisher scientific, cat. no. L3224) were resuspended in 10 mL of PBS. After 30 min in the dark at room temperature as manufacturer'instruction, the solution was filtered with Amicon Pro filters (10,000 kDa, Merck KGaA, cat. no. ACS500312) and centrifuged at 4000 rpm, 4 °C for 30 min. The concentrated solution with Calcein AM-labeled MBVs was resuspended in basal cell media and immediately added to cells.

DiI (1, 1′-dioctadecyl-3, 3, 3′, 3′-tetramethyl indocarbocyanine perchlorate) labeling:1×10^{10} MBVs were labeled with 60 μL of DiI (Invitrogen, Vybrant™ DiI Cell-Labeling Solution, cat. no. V22885, 1 μM) in a total volume of 2.5 mL of PBS. After one hour at 4 °C in the dark, PBS was added to a final volume of 10 mL. The solution was transferred to Amicon Pro filters (10,000 kDa, Merck KGaA) and centrifuged at 4 °C at 4000 rpm for 30 min. The concentrated solution with DiL-labeled MBVs was added to 4×10^4 IVD cells, previously seeded in 24-well plate.

For both staining, fluorescence images were obtained after 2 and 4 h of incubation at 37 °C with the Olympus IX71 microscope (Olympus Co., Tokyo, Japan).

2.8. Cell viability

For calcein AM/propidium iodide (PI) staining, IVD cells were seeded in a 24-well plate at density of 5000 cells/well, and were exposed to 1×10^9/mL of MBVs and cultured up to 7 days. Before staining, the medium was removed from the wells, and 500 μL staining solution (Merck KGaA) was added to each well. The samples were incubated in the dark at RT for 15 min, after which, the wells were rinsed with PBS and immediately visualized under a fluorescence microscope (Nikon Eclipse 50i, Nikon Corporation, Tokyo, Japan). Dead cells were stained red, whereas viable cells appeared green. Conversely, the proliferation rate of IVD cells cultured in the presence of MBVs was determined by the AlamarBlue® assay (cat.no. DAL1025, Thermo Fisher Scientific). Briefly, cells were plated at a density of 10,000 cells/cm^2, and exposed to MBVs up to 7 days. After different length of time, the ready-to-use resazurin-based solution was added to the cells. Following 4 h of incubation, 200 μL of the cell medium was transferred to a 96-well plate. The resorufin (reduced form) was then detected using fluorescence (Ex/Em 530–560/590 nm) with a microplate reader (Infinite 200, Tecan, Switzerland). The results were reported as relative fluorescence units (RFU) after normalization for protein content, determined by Bradford assay (Merck KGaA).

2.9. Phalloidin staining

To evaluate the shape and structure of the cells, IVD cells were seeded in 24-well plates (5000 cells/well), and were exposed to 1×10^9/mL of MBVs and cultured up to 7 days. Then, the cells were fixed with 4 % paraformaldehyde for 2 min at 37 °C and permeabilized with 0.2 % Triton X-100 in PBS for 15 min. The cells were then stained with Alexa Fluor 488 phalloidin (Thermo Fisher Scientific, 1:500 dilution in PBS) at RT in the dark for 30 min. Subsequently, the cells were washed with PBS and the nuclei were counterstained with DAPI® solution (Merck KGaA). Fluorescent images were obtained using a fluorescence microscope (Nikon Eclipse 50i).

2.10. Wound scratch assay

2.6×10^4 of IVD cells were resuspended in 100 μL of basal medium and seeded in each compartment of Ibidi insert (Ibidi, Gräfelfing, Germany; cat. no. 81176) within a 24-well plate. Once cells reached 100 % of confluence, the insert was removed and 500 μL of basal culture media was added in the presence (or absence, control cells) of 1×10^9 MBVs. The scratches were examined by the Olympus IX71 microscope (Olympus Co.). Images were captured at different time points until the complete closure of the scratch (80 h after wound generation). Experiments were performed in triplicate. The healing area was semi-quantified using ImageJ™ software (1.51p version; National Institutes of Health, USA) and the results are expressed as a percentage of wound

area.

2.11. Immunocytochemistry

Immunocytochemistry analysis was performed using the ImmPRESS kit (MP-7500; Vector Laboratories, Inc., Newark, CA, USA). IVD cells were plated at a density of 5000 cells/well in 96-well plates in the presence (or absence, control cells) of 1×10^9 MBVs/mL. After 7 days, IVD cells were fixed in cold 100 % methanol at RT for 10 min and permeabilized with 0.2 % (v/v) Triton X-100 (Merck KGaA) in 1× Tris-buffered saline (TBS) at RT for 10 min. Cells were treated with 3 % H_2O_2 in 1× TBS at RT for 10 min and incubated in 2 % normal horse serum (Vector Laboratories, Inc.) for 15 min at RT. After incubation in blocking serum, primary antibodies against SOX9 (ab5535, Merck KGaA, 1:500 dilution), TRPS1 (ProteinTech Group, Rosemont, IL, USA, 20003–1-AP, 1:100 dilution), COL2a1 (ab3092, Abcam, 1:200 dilution), FOXO3a (ab70315, Abcam, Cambridge, UK, 1:1000 dilution), were added and incubated at 4 °C overnight. After rinsing in 1× TBS, the cells were incubated for 30 min at RT with ImmPRESS-HRP Universal Polymer reagent (horse anti-mouse/rabbit IgG) and then stained with substrate/chromogen mix (ImmPACT™ DAB) for 5 min at RT. After washing, the cells were mounted in glycerol/PBS (9:1) and observed under a Nikon Eclipse 50i optical microscope. Semi-quantitative image analysis of immunostained cells was performed using ImageJ™ software as previously reported (Penolazzi et al., 2018).

2.12. MBVs growth factors profiling

MBVs were lyophilized overnight using LIO-5PDGT (CDL, Padua, Italy) to minimize sample dilution during the protein extraction process. The protein extraction from the obtained MBVs pellet was carried out by adding 30 μL of RIPA buffer and incubating on ice, with pipetting at 10 min intervals over a total incubation period of 30 min. Protein content was obtained after centrifugation for 30 min at 4 °C and 13,000 rpm. The supernatant was collected and immediately used for further analyses. Total protein quantification was performed using the Pierce™ BCA Protein Assay Kit (Thermo Fisher Scientific). Human Growth Factors Array Q1 (QAH-GF-1, RayBiotech, GA, USA) was used to evaluate the presence of 40 different growth factors in MBVs' protein extracts. Briefly, capture antibodies were pre-spotted in quadruplicate on a histology glass slide, with each set corresponding to a specific analyte (see Table S1). A total of 50 μg of protein for each sample was used according to the manufacturer's protocol. The kit also included cytokine standards and negative controls to enable quantitative analysis. Additional internal control spots are embedded on the array, as specified by the manufacturer. Fluorescence intensity measurements and data quantification were performed by the manufacturer as part of their analysis service.

2.13. Global miRNA profiling: Library preparation, sequencing and data normalization

Total RNA was extracted from 690 μL of MBVs [1.28×10^{10}/mL] isolated from DWJ ($n = 3$) using the miRNeasy Mini Kit (QIAGEN, Hilden, Germany) in combination with TRIzol-LS Reagent (Thermo Fischer Scientific), applied in a volumetric ratio of 1:3. Fifty-two QIAseq miRNA Library QC Spike-Ins were added to the samples during RNA isolation. The total miRNAs were quantified using the Qubit™ microRNA Assay Kit (Thermo Fisher Scientific).

miRNA libraries were prepared with the QIAseq miRNA UDI Library Kit (QIAGEN), which incorporates Unique Molecular Index (UMI) technology. The libraries were subsequently amplified and purified. For quality control, 1 μL of the prepared libraries was analyzed on a TapeStation system using the High Sensitivity D1000 ScreenTape (Agilent Technologies Inc., CA, USA), and their concentrations were determined using the Qubit™ 1× dsDNA HS Assay Kit (Thermo Fisher Scientific). miRNA sequencing was performed on a NextSeq 500/550 system (Illumina, CA, USA) using single-end reads with dual indices (10 bp) and a 1 × 72 bp sequencing format, achieving a depth of 12–14 million reads per sample (v2.5 kits). FASTQ files were analyzed using the GeneGlobe Data Analysis Center, an online QIAGEN platform. The platform automatically aligns and reports on the QIAseq miRNA spike-ins in addition to the aligned small RNA, miRNA, and piRNA from the samples.

2.14. MSigDB analysis

The molecular signature database (MSigDB v7.0; UC San Diego, CA, USA, and Broad Institute, Boston, MA, USA) was interrogated to compute overlapping analysis of experimentally validated target genes for the seven common miRNAs retrieved from miRTar Base (version 8.0), with the Hallmark gene sets ($N = 50$) which represent "specific well-defined biological states or processes and display coherent expression" (Liberzon et al., 2015).

2.15. Statistical analysis

All experiments were performed at least in triplicate, each sample was tested 3–5 times, and all numerical data were expressed as mean ± SD. Statistical differences between groups were evaluated with Student's two-tailed unpaired *t*-test or two-way ANOVA and post-hoc Tukey's test. All statistics were performed using GraphPad's Prism software, release version 10. A value of $P \leq 0.05$ was considered statistically significant.

3. Results

3.1. MBVs are present in decellularized Wharton's jelly

MBVs were isolated from DWJ and characterized as described in the Materials and methods section and as reported in Fig. 1A. In particular, we paid attention to evaluate both the efficiency of decellularization of Wharton's Jelly post-DET by quantifying residual DNA (below the threshold of 50 ng/mg) and the maintenance of the native ECM fibrillary microstructure (Penolazzi et al., 2022).

Different MBVs preparations were subjected to nanoparticle tracking analysis (NTA) and tunable resistive pulse sensing (TRPS) to characterize particles concentration and size distribution. The NTA and TRPS profiles showed that most of the nanoparticles were about 150 nm in size and very similar in shape (Fig. 1B, C). Only a small percentage of the detected nanoparticles showed a shape/size ratio indicative of fused particles (data not shown), suggesting that ultracentrifugation-induced particle fusion was minimal. The presence of MBVs in different DWJ samples was confirmed using transmission electron microscopy (TEM) which highlighted rounded vesicular structures with diameters ranging from 100 to 300 nm (Fig. 1D) together with small rounded shapes of <50 nm around the nanoparticles. The latter should be considered artifacts, while the features of the former are consistent with those described in the literature regarding MBVs from several other tissues (Di Francesco et al., 2024).

MBVs were then characterized in terms of surface marker expression using Multiplex Bead-Based Flow Cytometry which ensures the exclusive detection of MBVs, excluding free proteins. As reported in Fig. 1E, isolated MBVs were positive for classical tetraspanin EV-associated biomarkers (CD9, CD63, and CD81) (Andreu and Yáñez-Mó, 2014). MBVs surface marker profile also revealed the presence of integrin alpha 2b (CD41b) and the pluripotency marker CD24, which suggests the role of MBVs in various cellular responses, such as immunomodulation and regeneration (Adorno-Cruz and Liu, 2018; Shakiba et al., 2015). The detectable level of a parental cell surface marker, such as CD29, suggests that during biogenesis, EVs are most likely to be invaginated from the parental cell membrane, significantly expressing CD29 (Holcar et al.,

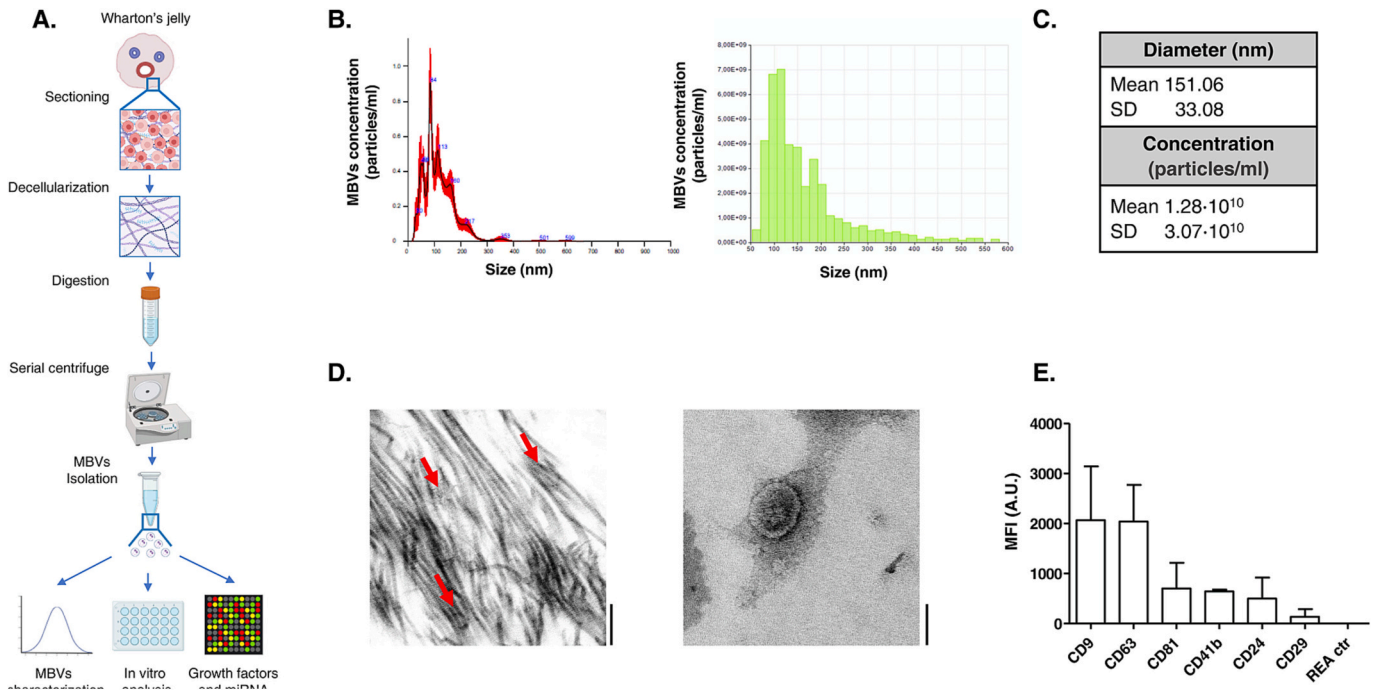

Fig. 1. MBVs characterization. (A) Brief overview of the MBVs isolation process from DWJ. (B) Representative Nanosight and qNano plots illustrating particle concentration and diameter size distribution. (C) Mean values of diameter and particle concentration (±SD, $n = 8$). (D) Representative TEM images of DWJ and MBVs fixed on carbon-coated grids. Red arrows highlighted MBVs entrapped in ECM, Bars: 500 nm (image on the left) and 100 nm (image on the right). E. Surface markers profiling of MBVs were obtained using multiplex bead-based flow cytometry assay. The 6 out 37 proteins that were found to be positive (MFI >50) in any of the MBVs samples ($n = 3$) are shown in the figure. All data reported and analyzed are expressed as units of background subtracted MFI (Net MFI - blank wells) ± SD. REA ctr: isotype control. (For interpretation of the references to colour in this figure legend, the reader is referred to the web version of this article.)

2025). Overall, the data collected so far on proteins characterizing the different MBVs preparations demonstrated, on the one hand, the consistency of the procedure applied to the different MBV samples, on the other hand the expected heterogeneity of MBVs populations. However, further investigation on MBV markers could demonstrate the presence of specific proteins that will be strictly correlated to the type of parental cells from which MBVs originate.

3.2. Anti-inflammatory property of MBVs when in contact with innate immune cells

The immunomodulatory capacity of different MBVs samples was analyzed by stimulating the production of pro-inflammatory cytokines and the consequent polarization of macrophages towards the M1 phenotype through exposure to LPS (Yunna et al., 2020). To this aim, firstly the MBVs were labeled with Calcein AM and their uptake was tested using the macrophage cell line RAW 264.7. As shown in Fig. 2A, Calcein AM-labeled MBVs were detected in the cytoplasm of macrophages after 4 h. Secondly, cells were stimulated with LPS promoting inducible nitric oxide synthase (iNOS) and producing large amounts of nitric oxide (NO), which was then effectively suppressed by dexamethasone treatment. When RAW 264.7 cells were exposed to MBVs from different preparations (tested at doses 1×10^8, 5×10^8, 1×10^9, and 5×10^9), the inhibition of nitrite production was comparable to that exerted by dexamethasone treatment (Fig. 2B).

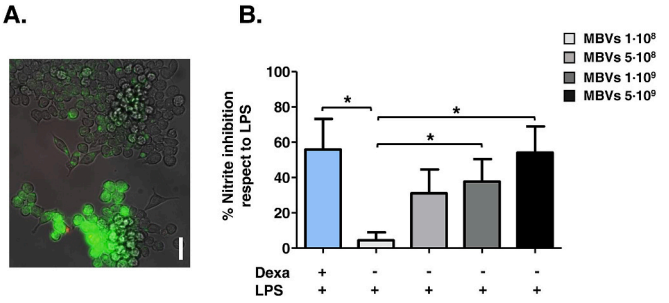

Fig. 2. Immunogenic responses of RAW 264.7 murine macrophages to MBVs. (A) Representative image showing cellular uptake of MBVs labeled with Calcein AM (green fluorescence), evaluated after 4 h in culture. (B) Inhibition of nitrite production in LPS-stimulated cells exposed (+) or not (−) to dexamethasone (Dexa, 1g/mL) and to increasing doses of MBVs, measured by the Griess assay. Data are shown as the mean ± SD. Statistical analysis was performed using the Student's two-tailed unpaired *t*-test and reported as $^*P < 0.05$ (n = 3). (For interpretation of the references to colour in this figure legend, the reader is referred to the web version of this article.)

3.3. Uptake of MBVs by IVD cells and cytocompatibility

Considering our final goal, we then moved on to evaluate the effect of MBVs on IVD cells from IVD biopsies with different levels of degeneration, using cells expanded at the P2 passage. As previously reported (Penolazzi et al., 2018), when IVD cells are expanded in culture they undergo de-differentiation which recapitulates the degeneration process by losing their chondrocyte-like phenotype, as revealed by the reduced expression of typical chondrogenic markers, including Aggrecan, Collagen-type II and the SOX9 transcription factor (Supplementary Fig. 1). Experiments we performed on these cells required a preliminary assay to choose the appropriate concentration of MBVs to expose the cells to. This was based on the evaluation of the modulation of the transcription factor SOX9 which is recognized as one of the main regulators of discogenic differentiation. As reported in Supplementary Fig. 2, the MBV dose of 1×10^9/mL significantly increased SOX9 expression after 7 days of exposure compared to lower doses.

In a first series of experiments, we demonstrated that, as reported in Fig. 3A, IVD cells showed a remarkable ability to uptake MBVs labeled

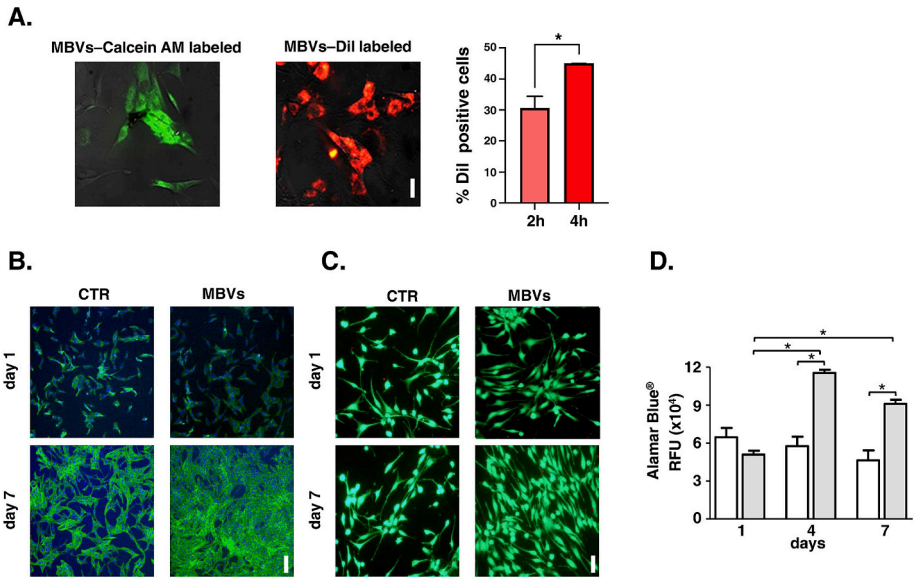

Fig. 3. Responses of IVD cells to MBVs: cellular uptake (A), morphology (B), viability (C) and cell proliferation (D). (A) Representative images showing cellular uptake of MBVs labeled with Calcein AM (green fluorescence, left) and Dil (red fluorescence, right), evaluated after 2 and 4 h in culture. Quantification of the percentage of Dil-positive cells compared to the total of IVD cells is also shown. Data are shown as the mean ± SD. Statistical analysis was performed using the Student's two-tailed unpaired t-test and reported as *P < 0.05 (n = 3).
(B, C) The cells in culture were exposed (MBVs) or not (CTR) to the MBV dose of 1×10^9/mL for the indicated times. (B) Cytoskeletal organization was analyzed by Alexa Fluor 488 Phalloidin staining and fluorescence microscope (Nikon Eclipse 50i). Representative images of the cells are reported. Nuclei were counterstained with DAPI® (blue fluorescence). The experiments were performed in triplicate. (C) The viability was monitored by double staining with Calcein AM/Propidium Iodide. The green fluorescence indicates the presence of Calcein labeled live cells, while propidium iodide labeled dead cells are revealed by red fluorescence. Merged representative photomicrographs are reported. Bars: 20 μm. (D) Cell proliferation was assessed by AlamarBlue® in IVD cells exposed to MBVs for a period of 7 days. The graph depicts the amount of relative fluorescence units normalized against protein content (RFU ± SD, $n = 6$. * $P < 0.001$; white columns, control cells; gray columns, MBVs-exposed cells). (For interpretation of the references to colour in this figure legend, the reader is referred to the web version of this article.)

with Calcein AM or with the lipophilic dye Dil after 2 and 4 h, without affecting cell morphology (Fig. 3B). MBVs treatment maintained viable cells (Fig. 3C and D), even inducing increased proliferation after four days in culture as demonstrated by the AlamarBlue® assay (Fig. 3D).

3.4. MBVs affect wound healing and IVD cells phenotype

The effects of the MBVs on cell motility were assessed through the wound scratch assay. A scratch was made in each well where IVD cells grew, and the wound closure was tracked up to 80 h. As reported in Fig. 4A, exposure of IVD cells to MBVs was significantly effective in inducing wound closure compared to control cells. Cell migration through the gap was already appreciable after 48 h, and complete wound closure was achieved after 80 h.

To investigate whether the MBVs were able to exert anabolic effects comparable to those of DWJ previously demonstrated by us (Penolazzi et al., 2024; Penolazzi et al., 2022), IVD cells at passage P2 were exposed to MBVs for 7 days, and the restoration of the native chondrocyte-like phenotype was monitored. Immunocytochemical analysis reported in Fig. 4B, showed a significant increase in the expression of SOX9 and TRPS1 and a non-significant change in FOXO3a and Collagen-type II.

Understanding the mechanisms by which MBVs exert their effect on IVD cells requires in-depth molecular characterization of their composition. In this regard, a preliminary investigation of the molecular signature upon the expression of growth factors and the miRNA content was performed.

We investigated 40 growth factors associated with different signaling pathways related to cell proliferation, differentiation and migration (Table S1, Fig. 5) and, in some contexts, to the ability to repair and regenerate damaged tissue. The more expressed factors (1500–9926 pg/100 g protein) were the morphogenetic protein 4 (BMP4), the basic fibroblast growth factor (bFGF), the Epidermal growth factor receptor (EGFR), the Insulin-like growth factor (IGF) binding proteins IGFBP2 and 4, and the vascular endothelial growth factor receptor 3 (VEGF-R3). Detectable levels (110–606 pg/100 g protein) were found for M-CSF-R, VEGF, IGFBP1, the growth hormone (GH), neurotrophins (NT3, NT4), osteoprotegerin (OPG), Heparin-binding EGF-like growth factor (HB-EGF), hepatocyte growth factor (HGF). Very low levels (below 110 pg/100 g protein) were found for VEGF-R2, stem cells factor (SCF) and its receptor (SCFR), Placental growth factor (PIGF), Platelet-derived growth factor (PDGF AA), Growth/differentiation factor-15 (GDF-15). Factors such as BMP5 and 7, epidermal growth factor (EGF), IGFBP-3, insulin, transforming growth factor (TGFa, TGFb1 and TGFb3) and anfiregulin (AR) were undetectable.

MBVs isolated from three different samples of DWJ were characterized for their miRNA content using next-generation sequencing (NGS). The Global miRNA profiling revealed that, among about one hundred miRNAs detected, a total of seven miRNAs were common expressed in MBVs isolated from DWJ (Fig. 6A-C; Table S2). A validated data set from miRTarBase has been used to identify genes that are targeted by miR-320a-3p, miR-143-3p, let-7b-5p, miR-335-5p, miR-382-5p, miR-574-5p, and let-7a-5p. For this purpose, only experimental validated target genes (strong evidence obtained by Western blotting, RT-qPCR or gene reporter assay) were reported (Fig. 6D).

Molecular Signature Database (MsigDB) analysis of the set of 164 experimentally validated target genes retrieved from miRTarBase for the seven common miRNAs isolated from MBVs underlined a significant enrichment gene set in apoptosis, cell cycle, remodeling and inflammatory pathways (Fig. 6E; Table S3).

4. Discussion

In the present study, the presence of matrix-bound vesicles (MBVs) in decellularized Wharton's jelly matrix (DWJ) from human umbilical cord was evaluated, along with their ability to influence the phenotype of degenerated human IVD cells. These MBVs appear to be associated with

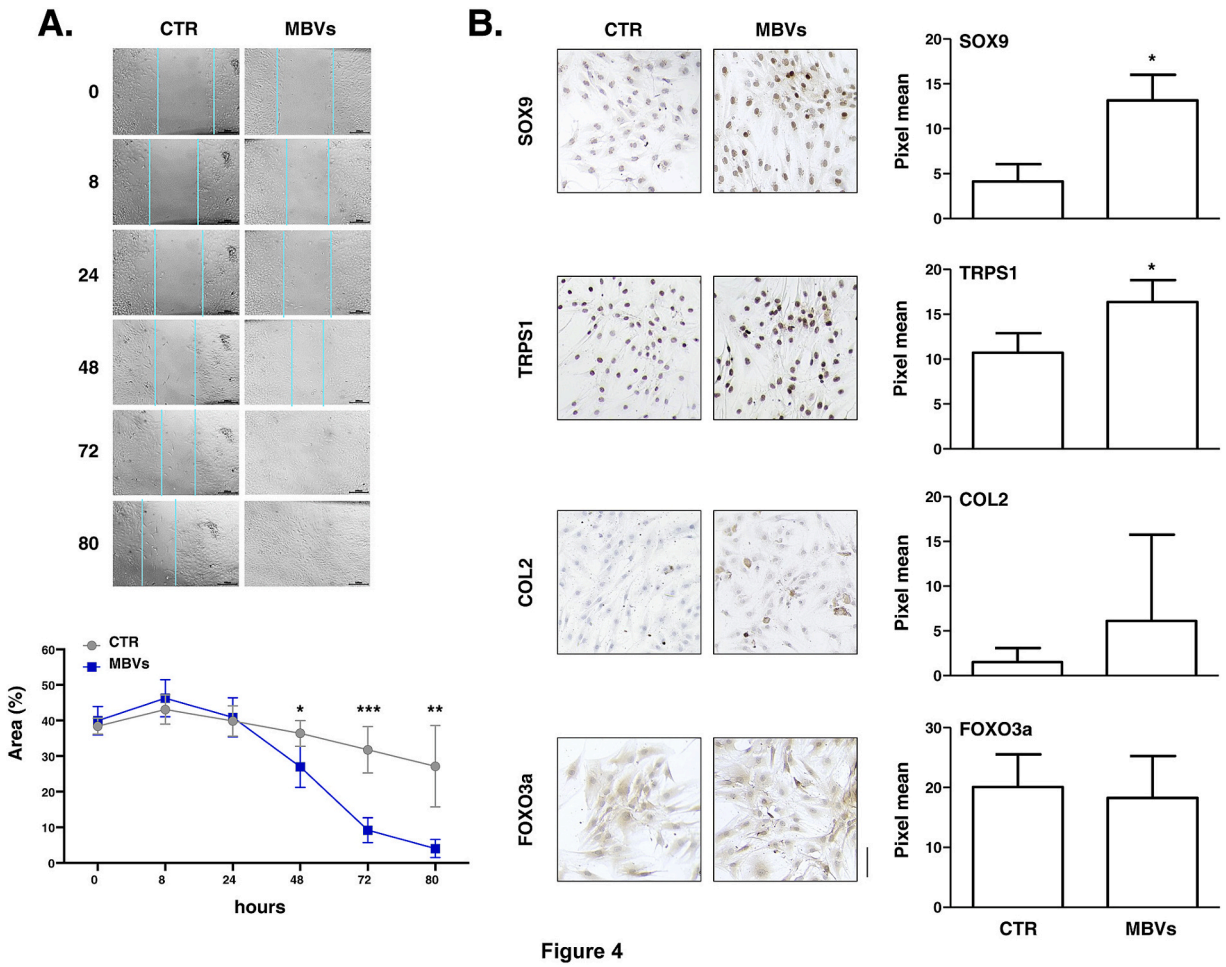

Fig. 4. Responses of IVD cells to MBVs: wound healing (A) and discogenic phenotype (B). The cells in culture were exposed or not (CTR) to the MBV dose of 1×10^9/mL for the indicated times. (A)Wound scratch assay was performed at 0, 8, 24, 48, 72 and 80 h after exposure of the cells to MBVs. A representative wound scratch both in the presence (MBVs) or absence (CTR) of MBVs is reported. The experiments were performed in triplicate and expressed as mean percentage of wound area covered by the IVD cells along the experiment. (*$p < 0.05$ versus control; **$p < 0.01$ versus CTR; ***$p < 0.001$ versus CTR). (B) SOX9, TRPS1, COL2 and FOXO3a expression in IVD cells after 7 days of exposure to MBVs. The expression was evaluated by immunocytochemistry and representative photomicrographs are reported. Protein levels were quantified by densitometric analysis of immunocytochemical pictures using Fiji software and expressed as means of pixels per one hundred cells ± SD. Quantification was performed in quadruplicate on samples from 4 different donors. * $p < 0.05$ versus CTR. Statistical analysis by Student's t-test. Scale bar: 20 μm.

DWJ probably within collagen fibers that provide the vesicles with adequate protection from the agents/methods used for decellularization of the matrix. We demonstrated that these MBVs can induce changes in the behavior of IVD cells in culture without cytotoxic effects, inducing cell migration and increasing the expression of specific proteins (including SOX9, TRPS1 and Collagen type II) that are associated with restoration of the native healthy chondrocyte-like phenotype (Penolazzi et al., 2018). Moreover, we demonstrated the anti-inflammatory potential of DWJ-derived MBVs based on their ability to suppress the acquisition of the M1 phenotype in LPS-stimulated macrophages. This is consistent with evidence from studies proposing the use of stem cell-derived EVs as a promising cell-free strategy to treat IDD and enhance endogenous repair, also due to their anti-inflammatory properties (DiStefano et al., 2022; van Maanen et al., 2025; Li et al., 2022; Sun et al., 2021).

IVD cells we use come from degenerated disc tissue which, like all degenerated tissues, is characterized by the loss of ECM homeostasis (Taylor and Erwin, 2024; Zhang et al., 2022). It is known that the process of IVD degeneration is complex and multifactorial; however, as our understanding of the microenvironment of the degenerated IVD increases, potentially more targeted therapeutic approaches/strategies are proposed. In recent years, in the field of tissue engineering, the idea of developing simple systems inspired by what happens in nature is gaining ground among those studying innovative approaches for the treatment of degenerative diseases. This does not mean that the mimicking process is easy, as at least a couple of significant critical issues need to be taken into account, which are: a. the setup of an adequate experimental model and b. the development of methodologies capable to detect molecules/signals that, although powerfully and profoundly driving cellular behavior, are however quantitatively scarce. These considerations fit very well with the topic of the present study and the objectives we are pursuing, i.e. understanding the ways through which DWJ exerts its beneficial effects on a highly compromised microenvironment, such as the degenerated IVD. As previously demonstrated by us and many others, Wharton's jelly from human umbilical cord represents a valuable opportunity both from a technical and ethical point of view to obtain extracellular derivatives such as ECM, growth factors, and extracellular vesicles (Jadalannagari et al., 2017; Penolazzi et al., 2024; Penolazzi et al., 2022; Gupta et al., 2020; Bakhtyar et al., 2018; Fayon et al., 2022). After decellularization, no alterations were observed in the ECM components or in its physical and mechanical properties, thus obtaining a bioactive matrix suitable not only to act as a three-dimensional (3D) scaffold, but also to exert potential anabolic effects by supporting several cellular activities. In our hands DWJ alone or in a mixture with

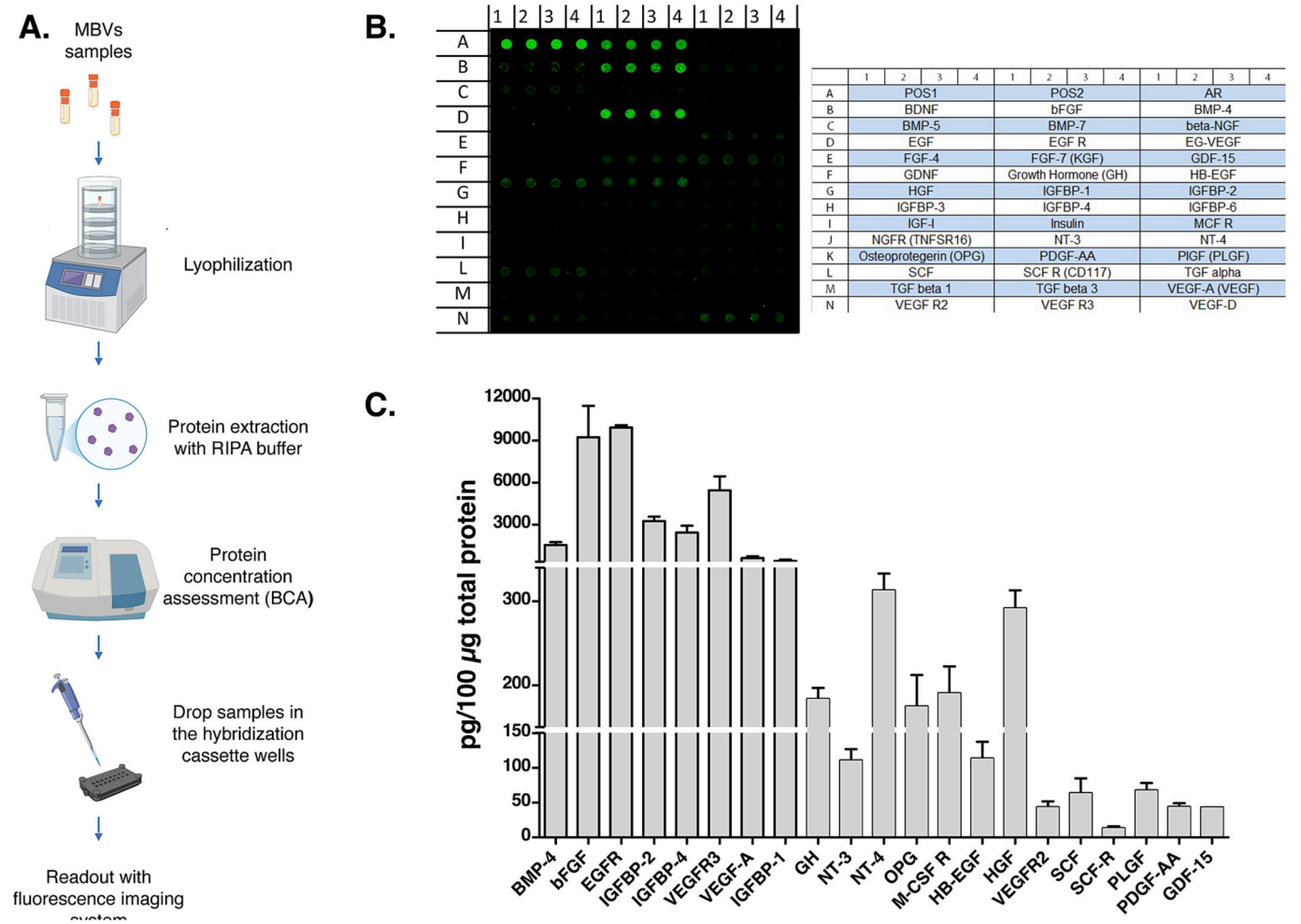

	1	2	3	4	1	2	3	4	1	2	3	4
A	POS1				POS2				AR			
B	BDNF				bFGF				BMP-4			
C	BMP-5				BMP-7				beta-NGF			
D	EGF				EGF R				EG-VEGF			
E	FGF-4				FGF-7 (KGF)				GDF-15			
F	GDNF				Growth Hormone (GH)				HB-EGF			
G	HGF				IGFBP-1				IGFBP-2			
H	IGFBP-3				IGFBP-4				IGFBP-6			
I	IGF-I				Insulin				MCF R			
J	NGFR (TNFSR16)				NT-3				NT-4			
K	Osteoprotegerin (OPG)				PDGF-AA				PlGF (PLGF)			
L	SCF				SCF R (CD117)				TGF alpha			
M	TGF beta 1				TGF beta 3				VEGF-A (VEGF)			
N	VEGF R2				VEGF R3				VEGF-D			

Fig. 5. Quantification of growth factors content in MBVs cargo. Human growth factors were analyzed by Quantibody® Human Growth Factor Array 1 (QAH-GF-1_RayBiotech), following the process reported in part A of the figure. (B) The representative fluorescence image of the MBVs sample loaded in the array is reported together with the scheme; each antibody is spotted in quadruplicate, with positive controls also indicated. (C) Results are showed as pg of the indicated protein relative to 100 µg of MBVs (total protein) ± SD ($n = 4$). The complete list and description of all analyzed proteins is provided in Table S1.

alginate and gelatin has proven effective in restoring the properties of human IVD cells lost following degeneration and inflammation of the disc tissue (Penolazzi et al., 2024; Penolazzi et al., 2022). The hypothesis that this effect may be mediated by MBVs present in the DWJ through their contribution to sustain cell-cell and cell-ECM communication and to promote the amplification of signaling useful for the maintenance of tissue homeostasis, is substantially confirmed by the data obtained here. It is therefore reasonable to think that the anabolic stimuli received by IVD cells when cultured in combination with DWJ and which support the reversal of IVD degeneration, are due not only to the 3D arrangement and bioactive molecules of a rich ECM, but also to the signaling potency of MBVs. To precisely delineate the functional role of these MBVs and their potential pro-discogenic effect, a thorough characterization of their nucleic acid, lipid and protein content will be necessary in the near future.

Our preliminary analysis suggests an interesting profile of MBVs cargo useful to study the molecular mechanisms by which DWJ-based scaffolds could modulate IVD cell behavior. For example, the results from the growth factors array limited to the detection of 40 factors deserve special attention for some of them, including BMP4 and bFGF. These factors more than others seem to play an important role in the regeneration process of various tissues including the intervertebral disc, by promoting cell proliferation and ECM anabolism (Pan et al., 2023; Beenken and Mohammadi, 2009). In particular, since BMP4 is known to positively regulate the master regulator of chondrogenesis, SOX9 (Dexheimer et al., 2016), BMP4-enhanced ECM deposition could occur via SOX9 in IVD cells expressing BMP receptors. Insulin-like growth factor (IGF) binding proteins, as components of the IGF system, have important effects on pathophysiology of multiple tissues by supporting cell migration and proliferation by inducing interactions with cells and the ECM (Hjortebjerg, 2018; Lin et al., 2022). Beyond any reasonable speculation, it is worth emphasizing that MBVs, being equipped with ligands and receptors, may participate in a communication system with the cell population in the IVD microenvironment and may be considered key players in supporting disc tissue regeneration processes by DWJ. This reasoning is also appropriate for miRNA profiling and for the seven miRNAs we identified (miR-320a-3p, miR-143-3p, let-7b-5p, miR-335-5p, miR-382-5p, miR-574-5p, and let-7a-5p) that are commonly expressed in MBVs from DWJ and may mainly regulate the expression of genes involved in apoptosis, cell cycle, remodeling and inflammatory pathways.

Another noteworthy aspect is the contribution our data can make to understanding the molecular mechanisms underlying the discogenic phenotype, which remain poorly understood to date. For this purpose, the data from our analysis need to be compared with literature data investigating the role of specific miRNAs, in many cases controversial (Genedy et al., 2024), and functionally validated in our experimental model as we plan to do in future investigations. In this regard, it is worth

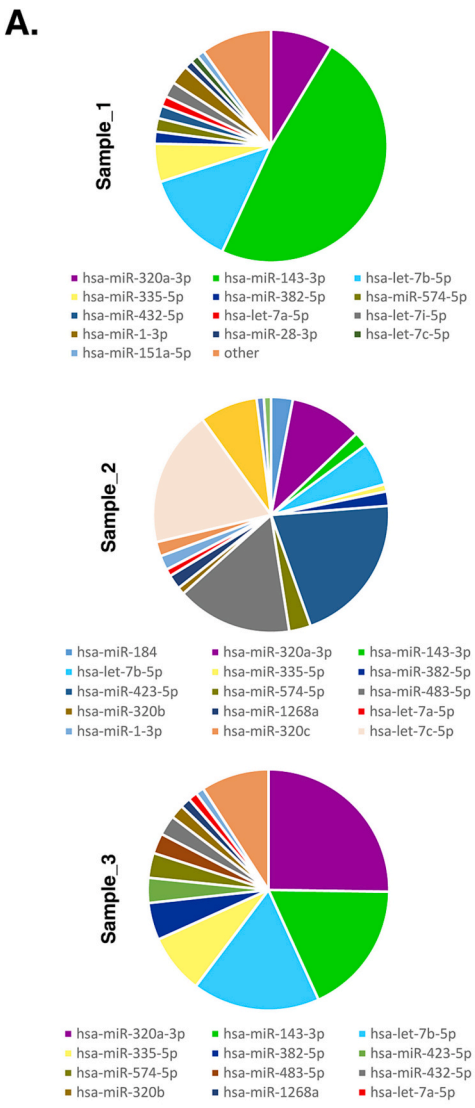

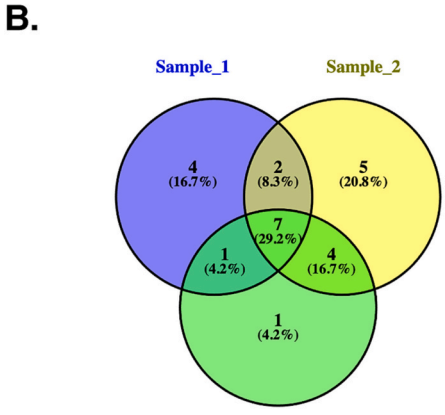

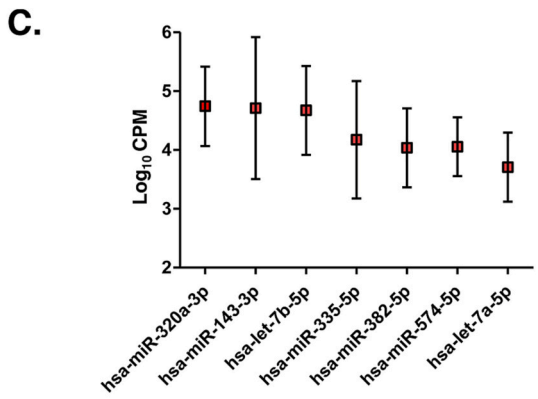

D.

	Validated target (Strong Evidences_miRTARbase)
hsa-miR-320a-3p	NPR1 MCL1 VDAC1 ITGB3 GNAI1 PDCD4 BMI1 ARF1 PBX3 NRP1 NFATC3 TRPC5 BANP RAB14 SUZ12 KITLG RUNX2 MTDH AQP4 AQP1 POLR3D TAC1 TFRC HSPB6 MAPK1
hsa-miR-143-3p	MACC1 KRAS MYO6 DNMT3A SERPINE1 FNDC3B MAPK7 HRAS FSCN1 HK2 PTGS2 JAG1 AKT1 BCL2 MMP13 SDC1 RREB1 CD44 KLF5 BRAF IGF1R GABARAPL1 NR2C2 IL13RA1 COL3A1 DDX6 LIMK1 NFATC1 COL1A1 MDM2 TNF HNF4A CTGF
hsa-let-7b-5p	CDC34 IGF2BP1 HMGA1 ANAPC1 HMGA2 CDC25A CDK6 CCND1 HRAS CCND2 NR2E1 IGF2BP2 PRDM1 CYP2J2 AGO1 IRS2 IGF1R TGFBR1 CTHRC1 AKT2 TNFRSF10B RDH10 MTPN RPIA ACTG1 LIN28B NRAS CCNA2 LIN28A IFNB1 NRAS CDC25A SCAMP3 HNRPDL PDGFRA BIRC6
hsa-miR-335-5p	MAPK1 TFF2 BCL2L2 LRG1 RASA1 RB1 RUNX2 DAAM1 BIRC5 FOXA2 SP1 MYC BRCA1 ID4 IGF1R EPN2 POU5F1 ROCK1 ZEB2 FMNL3 FMN2 DAAM2 SOX17 PARP1 TNC MERTK PTPRN2 SOX4 ARPC5L UBE2F
hsa-miR-382-5p	PTEN MXD1 NFIA YBX1 DRD1
hsa-miR-574-5p	FOXN3
hsa-let-7a-5p	CDK6 MYC NKIRAS2 ITGB3 NF2 NRAS KRAS PRDM1 RAVER2 HMGA2 EWSR1 HMGA1 E2F1 UHRF2 DICER1 HRAS CASP3 CASP8 CASP9 IL6 E2F2 CCND2 CDC34 IGF2BP1 CCR7 TMED7 CDKN1A RRM2 AGO1 EZH2 UHRF1 PAK1 AURKB RAB40C ARG2 TNFRSF10B MPL CDC25A BCL2 TRIM71 FOXA1 NR1I2 VDR EIF2C4 APP IGF2 LIN28A NFKB1 ZFP36L1 THBS1 TUSC2 SLC20A1 NEFM MEIS1 EGR3 HNRPDL AMMECR1 HAS2 EGFR

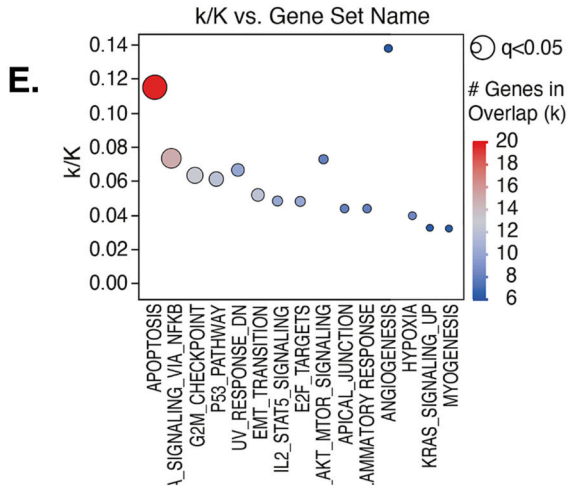

Fig. 6. Global miRNA profiling of MBVs isolated from three different samples of DWJ. (A) The relative abundance distribution of miRNAs (mean CPM $\geq$ 1 % as cutoff) across the MBVs samples from DWJ. (B) Venn diagram representing the overlap of expressed miRNA in MBVs samples from DWJ. (C) The graph displays the seven-miRNA quantification expressed as log10 CPM (n = 3, mean $\pm$ SD). (D) Experimentally validated target genes were retrieved from miRTar Base (version 8.0) for the seven common expressed miRNAs in DWJ. (E) MSigDB analysis of the experimentally validated target genes for the seven miRNAs with the Hallmark (H) gene sets (N = 50). The bubble plot shows the top 15 overlapping gene sets among miRNA regulated genes. Bubble size represents statistical significance of overlap expressed as -log10 (q-value), where the larger the size the greater the significance. In X-axis, H-gene set name; in Y-axes, the ratio of overlap (k/K) is shown where 'k' represent the number of miRNAs regulated genes while 'K' the number of genes in the specific H-gene set. Bubble colour reflects the number of miRNA Target genes (k). The complete results are provided in Table S3. CPM = count per million.

highlighting, for example, that miR-320a-3p and miR-335-5p can protect cartilage from degradation and inflammation by targeting the transcription factor RUNX2 or TNF-α which is highly expressed in hypertrophic chondrocytes and in degenerated IVD cells (Peng et al., 2017; Zhong et al., 2019). miR-143-3p was found to regulate early cartilage differentiation and contribute to cartilage damage repair through targeting BMPR2 (Tian et al., 2018). Conversely, other studies suggest that miR-143-3p has different regulatory roles, for example demonstrating that it inhibits the transcriptional activity of SOX5 through targeted binding, thus inducing IDD (Gao et al., 2022). Interestingly, MBVs from DWJ do not contain miRNA-221, which, as previously demonstrated by us and others, is among the most potent negative regulators of chondrogenesis (Penolazzi et al., 2018), nor miR-338-3p, which is markedly increased in human IDD (Jiang et al., 2021).

Clearly, the maintenance of IVD homeostasis, as well as the onset of disc degeneration, are the result of the combination of numerous regulatory molecules whose activity is strongly influenced by continuous intra- and extra-cellular changes. Therefore, investigating in more detail the critical biomolecular components of MBVs will provide a more detailed and in-depth understanding of the IVD microenvironment and pave the way for the development of new strategies to treat IDD. Indeed, regarding the therapeutic potential of DWJ-derived MBVs, as well as that of EVs in general (Turner et al., 2022; Debnath et al., 2023; Kim et al., 2024; Mazahir and Yadav, 2024; DiStefano et al., 2022), it will be essential in the near future not only to optimize the manufacturing process, but also to understand the mechanisms mediating their different actions, which, in our case, appear to converge in a pro-discogenic effect.

Supplementary data to this article can be found online at https://doi.org/10.1016/j.yexmp.2025.105011.

CRediT authorship contribution statement

Letizia Penolazzi: Writing – review & editing, Validation, Methodology, Data curation. **Alice Zaramella:** Validation, Methodology, Investigation, Data curation. **Anna Chierici:** Methodology, Investigation, Formal analysis. **Paola Bisaccia:** Methodology, Investigation, Formal analysis. **Maria Pina Notarangelo:** Methodology, Investigation, Formal analysis. **Anna Maria Tolomeo:** Methodology, Investigation, Formal analysis. **Elisabetta Lambertini:** Methodology, Investigation, Formal analysis. **Anna Alessia Saponaro:** Methodology, Investigation, Formal analysis. **Tommaso Colangelo:** Writing – review & editing, Conceptualization. **Michela Pozzobon:** Writing – review & editing, Funding acquisition, Conceptualization. **Roberta Piva:** Writing – review & editing, Writing – original draft, Validation, Supervision, Resources, Project administration, Funding acquisition, Data curation, Conceptualization.

Ethics approval and consent to participate

Human umbilical cords were collected from newborns after mothers' understanding and written informed consent and approval of the Ethics Committee of the University of Ferrara and S. Anna Hospital (protocol no. 061199/AOUFe). Human lumbar IVD tissues were collected as surgical waste from patients undergoing surgical discectomy after approval of the Ethics Committee of the University of Ferrara and University S. Anna Hospital (protocol no. 160998/AOUFe), and written informed consent from each patient (in full accordance with the Declaration of Helsinki).

Funding

This work was supported by PRIN 2022 (code 2022RHHFCX, funded by European Union - Next Generation EU), Interuniversity Consortium for Biotechnologies, Italy (C.I.B.) (CIB-Unife-2023 to R.P.), and Fondo di Ateneo per la Ricerca Scientifica (FAR 2024 grants to R.P. and L.P.).

Declaration of competing interest

The authors declare that they have no known competing financial interests or personal relationships that could have appeared to influence the work reported in this paper.

Acknowledgments

The authors thank Prof. Pasquale De Bonis and Dr. Chiara Angelini (Department of Neurosurgery, University Hospital of Ferrara) for IVD biopsy recruitment; Prof. Pantaleo Greco (Obstetrics and Gynecology Unit, Department of Medical Sciences, University of Ferrara) for umbilical cord recruitment; Dr. Paola Boldrini and Dr. Edi Simoni (Center for Electron Microscopy, University of Ferrara) for TEM analysis support; Dr. Cristina Manfrinato (Department of Chemical, Pharmaceutical and Agricultural Sciences, University of Ferrara) for her willingness to use fluorescence-based instrumentation.

Data availability

The datasets generated during and/or analyzed during the present study are available from the corresponding authors on reasonable request.

References

Adorno-Cruz, V., Liu, H., 2018. Regulation and functions of integrin α2 in cell adhesion and disease. Genes Dis. 6, 16–24. https://doi.org/10.1016/j.gendis.2018.12.003.
Andreu, Z., Yáñez-Mó, M., 2014. Tetraspanins in extracellular vesicle formation and function. Front. Immunol. 5 (442). https://doi.org/10.3389/fimmu.2014.00442.
Bakhtyar, N., Jeschke, M.G., Herer, E., Sheikholeslam, M., Amini-Nik, S., 2018. Exosomes from acellular Wharton's jelly of the human umbilical cord promotes skin wound healing. Stem Cell Res. Ther. 9 (193). https://doi.org/10.1186/s13287-018-0921-2.
Beenken, A., Mohammadi, M., 2009. The FGF family: biology, pathophysiology and therapy. Nat. Rev. Drug Discov. 8, 235–253. https://doi.org/10.1038/nrd2792.
Converse, G.L., Li, D., Buse, E.E., Hopkins, R.A., Aljitawi, O.S., 2018. Wharton's jelly matrix Decellularization for tissue engineering applications. Methods Mol. Biol. 1577, 25–33. https://doi.org/10.1007/7651_2017_61.
Debnath, K., Heras, K.L., Rivera, A., Lenzini, S., Shin, J.W., 2023. Extracellular vesicle-matrix interactions. Nat. Rev. Mater. 8, 390–402. https://doi.org/10.1038/s41578-023-00551-3.
Dexheimer, V., Gabler, J., Bomans, K., Sims, T., Omlor, G., Richter, W., 2016. Differential expression of TGF-β superfamily members and role of Smad1/5/9-signalling in chondral versus endochondral chondrocyte differentiation. Sci. Rep. 6 (36655). https://doi.org/10.1038/srep36655.
Di Francesco, D., et al., 2024. Characterisation of matrix-bound Nanovesicles (MBVs) isolated from Decellularised bovine pericardium: new Frontiers in regenerative medicine. Int. J. Mol. Sci. 25 (740). https://doi.org/10.3390/ijms25020740.
DiStefano, T.J., Vaso, K., Danias, G., Chionuma, H.N., Weiser, J.R., Iatridis, J.C., 2022. Extracellular vesicles as an emerging treatment option for intervertebral disc degeneration: therapeutic potential, translational pathways, and regulatory considerations. Adv. Healthc. Mater. 11, e2100596. https://doi.org/10.1002/adhm.202100596.
Dubus, M., et al., 2022. Decellularization of Wharton's jelly increases its bioactivity and antibacterial properties. Front. Bioeng. Biotechnol. 10 (828424). https://doi.org/10.3389/fbioe.2022.828424.
Elmounedi, N., Bahloul, W., Keskes, H., 2024. Current therapeutic strategies of intervertebral disc regenerative medicine. Mol. Diagn. Ther. 28, 745–775. https://doi.org/10.1007/s40291-024-00729-7.
EV-TRACK Consortium, 2017. EV-TRACK: transparent reporting and centralizing knowledge in extracellular vesicle research. Nat. Methods 14, 228–232. https://doi.org/10.1038/nmeth.4185.
Fayon, A., et al., 2022. Characterization of an innovative biomaterial derived from human Wharton's jelly as a new promising coating for tissue engineering applications. Front. Bioeng. Biotechnol. 10, 884069. https://doi.org/10.3389/fbioe.2022.884069.
Gao, D., Hu, B., Ding, B., Zhao, Q., Zhang, Y., Xiao, L., 2022. N6-Methyladenosine-induced miR-143-3p promotes intervertebral disc degeneration by regulating SOX5. Bone 163 (116503). https://doi.org/10.1016/j.bone.2022.116503.
Genedy, H.H., et al., 2024. MicroRNA-targeting nanomedicines for the treatment of intervertebral disc degeneration. Adv. Drug Deliv. Rev. 207 (115214). https://doi.org/10.1016/j.addr.2024.115214.
Gupta, A., El-Amin 3rd, S.F., Levy, H.J., Sze-Tu, R., Ibim, S.E., Maffulli, N., 2020. Umbilical cord-derived Wharton's jelly for regenerative medicine applications. J. Orthop. Surg. Res. 15 (49). https://doi.org/10.1186/s13018-020-1553-7.
Hjortebjerg, R., 2018. IGFBP-4 and PAPP-A in normal physiology and disease. Growth Hormon. IGF Res. 41, 7–22. https://doi.org/10.1016/j.ghir.2018.05.002.

Holcar, M., et al., 2025. Comprehensive phenotyping of extracellular vesicles in plasma of healthy humans - insights into cellular origin and biological variation. J. Extracell. Vesicles 14 (e70039). https://doi.org/10.1002/jev2.70039.
Huleihel, L., et al., 2016. Matrix-bound nanovesicles within ECM bioscaffolds. Sci. Adv. 2, e1600502. https://doi.org/10.1126/sciadv.1600502.
Jadalannagari, S., et al., 2017. Decellularized Wharton's Jelly from human umbilical cord as a novel 3D scaffolding material for tissue engineering applications. PLoS One 12. https://doi.org/10.1371/journal.pone.0172098.
Jiang, H., Moro, A., Wang, J., Meng, D., Zhan, X., Wei, Q., 2021. MicroRNA-338-3p as a novel therapeutic target for intervertebral disc degeneration. Exp. Mol. Med. 53, 1356–1365. https://doi.org/10.1038/s12276-021-00662-3.
Kim, H.I., Park, J., Zhu, Y., Wang, X., Han, Y., Zhang, D., 2024. Recent advances in extracellular vesicles for therapeutic cargo delivery. Exp. Mol. Med. 56, 836–849. https://doi.org/10.1038/s12276-024-01201-6.
Kobayashi, M., et al., 2022. Extraction and biological evaluation of matrix-bound Nanovesicles (MBVs) from high-hydrostatic pressure-Decellularized tissues. Int. J. Mol. Sci. 23 (8868). https://doi.org/10.3390/ijms23168868.
Li, W., Xu, Y., Chen, W., 2022. Bone mesenchymal stem cells deliver exogenous lncRNA CAHM via exosomes to regulate macrophage polarization and ameliorate intervertebral disc degeneration. Exp. Cell Res. 421 (2), 113408. https://doi.org/10.1016/j.yexcr.2022.113408.
Liberzon, A., Birger, C., Thorvaldsdóttir, H., Ghandi, M., Mesirov, J.P., Tamayo, P., 2015. The Molecular Signatures Database (MSigDB) hallmark gene set collection. Cell. Syst. 1, 417–425. https://doi.org/10.1016/j.cels.2015.12.004.
Lin, H., et al., 2022. IGF signaling in intervertebral disc health and disease. Front. Cell. Dev. Biol. 9, 817099. https://doi.org/10.3389/fcell.2021.817099.
Malvicini, R., et al., 2022. Macrophage bioassay standardization to assess the anti-inflammatory activity of mesenchymal stromal cell-derived small extracellular vesicles. Cytotherapy 24, 999–1012. https://doi.org/10.1016/j.jcyt.2022.05.011.
Mazahir, F., Yadav, A.K., 2024. Recent progress in engineered extracellular vesicles and their biomedical applications. Life Sci. 350, 122747. https://doi.org/10.1016/j.lfs.2024.122747.
Mohd Isa, I.L., Teoh, S.L., Mohd Nor, N.H., Mokhtar, S.A., 2022. Discogenic low Back pain: anatomy, pathophysiology and treatments of intervertebral disc degeneration. Int. J. Mol. Sci. 24 (208). https://doi.org/10.3390/ijms24010208.
Pan, Y., et al., 2023. Role and mechanism of BMP4 in regenerative medicine and tissue engineering. Ann. Biomed. Eng. 51, 1374–1389. https://doi.org/10.1007/s10439-023-03173-6.
Peng, H., Liang, D., Li, B., Liang, C., Huang, W., Lin, H., 2017. MicroRNA-320a protects against osteoarthritis cartilage degeneration by regulating the expressions of BMI-1 and RUNX2 in chondrocytes. Pharmazie 72, 223–226. https://doi.org/10.1691/ph.2017.6890.
Penolazzi, L., et al., 2018. MicroRNA-221 silencing attenuates the degenerated phenotype of intervertebral disc cells. Aging (Albany NY) 10, 2001–2015. https://doi.org/10.18632/aging.101525.
Penolazzi, L., et al., 2022. Decellularized extracellular matrix-based scaffold and hypoxic priming: A promising combination to improve the phenotype of degenerate intervertebral disc cells. Life Sci. 301 (120623). https://doi.org/10.1016/j.lfs.2022.120623.
Penolazzi, L., et al., 2023. Unorthodox localization of P2X7 receptor in subcellular compartments of skeletal system cells. Front. Cell. Dev. Biol. 11, 1180774. https://doi.org/10.3389/fcell.2023.1180774.
Penolazzi, L., et al., 2024. Wharton's jelly-derived multifunctional hydrogels: new tools to promote intervertebral disc regeneration in vitro and ex vivo. J. Biomed. Mater. Res. A 112, 973–987. https://doi.org/10.1002/jbm.a.37683.
Piening, L.M., Wachs, R.A., 2023. Matrix-bound Nanovesicles: what are they and what do they do? Cells Tissues Organs 212, 111–123. https://doi.org/10.1159/000522575.
Raposo, G., Stoorvogel, W., 2013. Extracellular vesicles: exosomes, microvesicles, and friends. J. Cell Biol. 200, 373–383. https://doi.org/10.1083/jcb.201211138.
Safari, F., Fani, N., Eglin, D., Alini, M., Stoddart, M.J., Baghaban Eslaminejad, M., 2019. Human umbilical cord-derived scaffolds for cartilage tissue engineering. J. Biomed. Mater. Res. A 107, 1793–1802. https://doi.org/10.1002/jbm.a.36698.
Samanta, A., Lufkin, T., Kraus, P., 2023. Intervertebral disc degeneration-current therapeutic options and challenges. Front. Public Health 11 (1156749). https://doi.org/10.3389/fpubh.2023.1156749.
Shakiba, N., et al., 2015. CD24 tracks divergent pluripotent states in mouse and human cells. Nat. Commun. 6 (7329). https://doi.org/10.1038/ncomms8329.
Sun, Z., et al., 2021. AF cell derived exosomes regulate endothelial cell migration and inflammation: implications for vascularization in intervertebral disc degeneration. Life Sci. 265, 118778. https://doi.org/10.1016/j.lfs.2020.118778.
Taylor, W., Erwin, W.M., 2024. Intervertebral disc degeneration and regeneration: new molecular mechanisms and therapeutics: obstacles and potential breakthrough technologies. Cells 13 (2103). https://doi.org/10.3390/cells13242103.
Tian, J., Rui, Y.J., Xu, Y.J., Zhang, S.A., 2018. MiR-143-3p regulates early cartilage differentiation of BMSCs and promotes cartilage damage repair through targeting BMPR2. Eur. Rev. Med. Pharmacol. Sci. 22, 8814-8821. Doi:10.26355/eurrev_201812_16649.
Turner, N.J., Quijano, L.M., Hussey, G.S., Jiang, P., Badylak, S.F., 2022. Matrix bound Nanovesicles have tissue-specific characteristics that suggest a regulatory role. Tissue Eng. Part A 28, 879–892. https://doi.org/10.1089/ten.tea.2022.0091.
van Maanen, J.C., et al., 2025. Explorative study of modulatory effects of notochordal cell-derived extracellular vesicles on the IL-1β-induced catabolic cascade in nucleus pulposus cell pellets and explants. JOR Spine 8 (1), e70043. https://doi.org/10.1002/jsp2.70043.
Yunna, C., Mengru, H., Lei, W., Weidong, C., 2020. Macrophage M1/M2 polarization. Eur. J. Pharmacol. 877, 173090. https://doi.org/10.1016/j.ejphar.2020.173090.
Zhang, S., et al., 2022. Extracellular matrix in intervertebral disc: basic and translational implications. Cell Tissue Res. 390, 1–22. https://doi.org/10.1007/s00441-022-03662-5.
Zhong, G., Long, H., Ma, S., Shunhan, Y., Li, J., Yao, J., 2019. miRNA-335-5p relieves chondrocyte inflammation by activating autophagy in osteoarthritis. Life Sci. 226, 164–172. https://doi.org/10.1016/j.lfs.2019.03.071.